Received: 19 May 2020 | Revised: 15 June 2020 | Accepted: 24 June 2020

DOI: 10.1111/ffe.13308

ORIGINAL CONTRIBUTION

FFEMS Fatigue & Fracture of Engineering Materials & Structures WILEY

Extension of the strain energy density method for fatigue assessment of welded joints to sub-zero temperatures

Moritz Braun[1] | **Claas Fischer**[2] | **Wolfgang Fricke**[1] | **Sören Ehlers**[1]

[1]Institute for Ship Structural Design and Analysis, Hamburg University of Technology, Hamburg, Germany

[2]Certification Renewables, TÜV NORD EnSys GmbH & Co. KG, Hamburg, Germany

Correspondence
Moritz Braun, Institute for Ship Structural Design and Analysis, Hamburg University of Technology, Am Schwarzenberg Campus 4(C), D-21073 Hamburg, Germany.
Email: moritz.br@tuhh.de

Funding information
Bundesministerium für Wirtschaft und Energie, Grant/Award Number: 03SX465B; German Federal Ministry for Economic Affairs and Energy, Grant/Award Number: 03SX465B
Open access funding enabled and organized by Projekt DEAL.

Abstract

Within stress-based fatigue assessment concepts, causes that do not influence the fatigue stress parameters, such as temperature, can only be accounted for by means of modification factors. The strain energy density (SED) method allows to account for changing material support effects and Young's modulus with temperature directly. Thus, in this study, a concept is presented to extend the SED method for fatigue assessment of welded joints at sub-zero temperatures. For this purpose, fatigue test results of welded joints made from normal and high-strength structural steel are assessed in the range of 20°C down to −50°C. The results are evaluated based on the formula that is used to derive the SED control radii of welded joints and compared with results of studies on SED-based assessment of notched components at high temperatures. From the estimates of the control radii, a temperature modification function for SED is derived for design purposes.

KEYWORDS

strain energy density, low temperatures, temperature dependence of fatigue curves, high-strength steel, weldment fatigue

1 | INTRODUCTION

Due to the increased interest in transarctic shipping and oil and gas exploration in the Arctic, several studies have been conducted in order to ensure safe operations of ships and offshore structures in Arctic regions.[1] One major knowledge gap reported for engineering structures exposed to Arctic conditions is the sub-zero temperature fatigue strength of welded joints.[2] In a recent publication, several stress-based fatigue assessment methods were applied to fatigue test results obtained for welded joints at sub-zero temperatures.[3] Beside large differences in prediction accuracy, significant problems arise from causes that do not directly influence the respective stresses. Typical example are thickness[4] or temperature effects[3] as well as postweld treatment.[5–7] For such effects, modification factors need to be applied in stress-based fatigue assessment methods or methods that take into account material support effects such as the stress averaging or critical distance approach.[8] Alternatively, the strain energy density (SED) method allows to take directly into account material support effects and changes of Young's modulus with temperature.

The SED concept has originally been derived from the notch stress intensity factor (N-SIF) concept. Based on the assumption of the weld toe and weld root being a V-notch without radius, the N-SIF can be derived from William's equations.[9] It can be shown that for an opening angle $2\alpha = 0°$, the N-SIF corresponds to stress intensity factor of a planar crack with depth equal to

the slit length.[10] Since the calculation of the N-SIF requires extremely refined finite element (FE) meshes, the SED concept was derived from the N-SIF concept and has successfully been applied to fatigue and fracture problems. Instead of analysing the stress in way of the notch tip, the SED is averaged $\bar{W}$ in a control volume around the notch tip. The deformation energy required for crack initiation in a unit volume of material was proposed by Gillemot[11] and Sih[12] around the same time. In general, the underlying idea is to account for the support of the material surrounding a local stress raiser like notches or cracks by assessing the strain energy in a short distance around the singularity. The SED concept has thus been applied to fatigue, ductile and brittle fracture alike. Moreover, it has successfully been applied to assess changes in fatigue and fracture strength of notched components at high temperatures.[13–16]

To the author's knowledge, the fatigue strength of welded joints at temperatures different from room temperature (RT) has so far only been assessed using stress-based concepts and modification factors. No study tried to incorporating temperature effects based on changes of material parameter and support effects into the assessment procedure for welded joints, yet. Thus, in this study, the fatigue strength of welded joints at sub-zero temperatures will be analysed by means of the SED method. For this purpose, a general introduction to the SED method will be given in Section 2.1, followed by some remarks to the application to welded joints (Section 2.2) and a summary of applications of the SED method to high-temperature fatigue assessment due to its similar but opposite effect on fatigue strength. In Section 3, fatigue test results of welded joints at sub-zero temperatures are presented, and in Section 4, a concept of taking into account temperatures within the SED method is introduced and subsequently evaluated.

2 | SED METHOD

2.1 | Background on the SED method

The two major benefits of the SED method are the underlying physical relation to the material fracture behaviour and that the SED averaged over a small size control volume surrounding the point of stress singularity is only slightly influenced by the mesh pattern.[17] Based on the Kitagawa-Takahashi diagram[18] and the relation between small and long cracks, Atzori and Lazzarin[19] derived a diagram for notches under Mode I loading and high cycle fatigue by substituting the theoretical stress concentration factors used for blunt notches by the N-SIF. That idea was then extended to fatigue assessment of welded joints with sharp notches at weld toe and weld root.

Lazzarin and Tovo showed that this N-SIF can be used as fatigue parameter for the life prediction of cyclically loaded welded joints and derived a corresponding stress-life (S–N) design curve from hundreds of fatigue tests.[10] The same data was later used to derive an SED-life ($\bar{W}-N$) design curve for welded joints.[20] Similarly to stress-life approaches, failure is assumed to occur when the SED range $\Delta\bar{W}$ reaches the critical value in a characteristic volume of the material. In the following paragraphs, the background of the SED method will be introduced for notches and then extended to welded joints.

Considering only the leading order terms of William's solution, the total elastic SED $\bar{W}$ averaged over the area defined by the control radius R_C (see Figure 1) is calculated by the following:

$$\bar{W} = \frac{e_1}{E}\left[\frac{K_1}{R_c^{1-\lambda_1}}\right]^2 + \frac{e_2}{E}\left[\frac{K_2}{R_c^{1-\lambda_2}}\right]^2, \quad (1)$$

where K_1 and K_2 are the N-SIF for modes I and II, E is the Young's modulus and e_1 and e_2 are correction factors, which depend on the stress-strain field (plane stress/plane strain), notch opening angle 2α and Poisson's ratio ν. Lazzarin and Zambardi[21] provide the following formulas for $\nu = 0.3$ under plane strain condition:

$$e_1 = -5.373\times10^{-6}(2\alpha)^2 + 6.151\times10^{-4}(2\alpha) + 0.133, \quad (2)$$

$$e_2 = 4.809\times10^{-6}(2\alpha)^2 - 2.346\times10^{-3}(2\alpha) + 0.34. \quad (3)$$

The parameters λ_1 and λ_2 are the eigenvalues of the Williams' stress field solution for the N-SIF K_1 and K_2 for modes I and II. The eigenvalues λ_1 and λ_2 can be derived from the following expressions:

$$\text{Mode I}: \sin(\lambda_1\gamma) = -\lambda_1 \times \sin(\gamma), \quad (4)$$

$$\text{Mode II}: \sin(\lambda_2\gamma) = \lambda_2 \times \sin(\gamma), \quad (5)$$

where $\gamma = 2\pi - 2\alpha$ is the angle between the notch bisector and the notch flanks.

Under plane strain condition, the control radius R_c depends on the fatigue limit of smooth base material specimen $\Delta\sigma_0$ and the fatigue crack growth threshold for long cracks ΔK_{th} as follows:

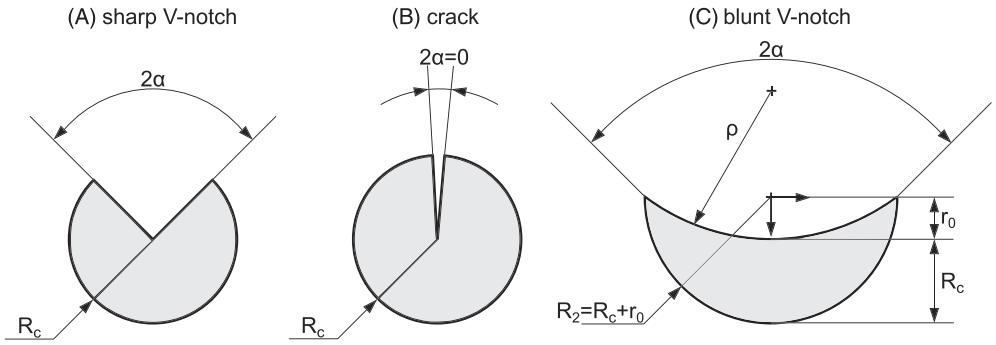

FIGURE 1 Critical volume (area) for (A) sharp V-notch, (B) crack, and (C) blunt V-notch adopted from Berto and Lazzarin.[22] Distance $r_0 = \rho(\pi - 2\alpha)/(2\pi - 2\alpha)$

$$R_C = \frac{(1+\nu)(5-8\nu)}{4\pi}\left(\frac{\Delta K_{th}}{\Delta\sigma_0}\right)^2. \quad (6)$$

Introducing the well-known El Haddad-Smith-Topper parameter a',[23] which can be used to predict the transition between short and long fatigue crack arrest, yields the following:

$$a' = \frac{1}{\pi}\left(\frac{\Delta K_{th}}{\Delta\sigma_0}\right)^2. \quad (7)$$

Under plane strain condition and if $\nu = 0.3$, Equation 6 becomes as follows:

$$R_C = 0.845a' \quad (8)$$

Thus, under Mode I loading, the control radius R_c is directly related to the crack arrest behaviour of the material, which is in turn described by the El Haddad-Smith-Topper parameter a'. Interestingly, the material characteristic length L, describing the material support effect, of Taylor's Theory of Critical Distance (TCD)[24]

$$L = \frac{1}{\pi}\left(\frac{\Delta K_{th}}{\Delta\sigma_0}\right)^2 \quad (9)$$

is thus directly related to the transition point between short and long crack growth ($a' = L$).[25] According to Radaj,[26] this relation only applies to stress ratios $R \geq 0$, since crack closure effects are not covered by the El Haddad-Smith-Topper parameter; however, for tensile loaded components, this relation allows to derive the control radius R_C from either El Haddad-Smith-Topper parameter a' or material characteristic length L. It will later be presented how this relation can be used to assess the fatigue strength at temperatures different from RT, but before that, an introduction to the fatigue assessment of welded joints by means of the SED method will be given.

2.2 | Application of the SED method to welded joints

Assuming sharp weld toe and root radii, Lazzarin et al[27] showed how the SED can be applied to assess the fatigue strength of welded joints, as presented in Figure 2. Here, σ_{rr}, $\sigma_{r\Theta}$ and $\sigma_{\Theta\Theta}$ are the stress components in polar coordinates (r, Θ) required to calculate Modes I and II N-SIF from William's equations.[9]

When constancy of the angle included between weld flanks and main plates is ensured and the angle is large enough to make Mode II contribution nonsingular, only Mode I NSIF K_1 is required to describe the fatigue strength of welded joints.[28] The control radius for weld toes and roots is thus determined by the following:

$$R_C = \left(\frac{\sqrt{2e_1}\times\Delta K_1^N}{\Delta\sigma_0}\right)^{\frac{1}{1-\lambda_1}}. \quad (10)$$

Herein, ΔK_1^N is the Mode I N-SIF fatigue strength for notched component (depends on the opening angle 2α) and $\Delta\sigma_0$ is the mean fatigue strength of plain specimens, that is, butt welds without notch (ground flush) for welded joints. For fatigue assessment of welded joints, both quantities have been derived for $R = 0$ and cycles to failure $N_f = 5 \times 10^6$. Based on $\Delta K_1^N = 211$ MPa mm$^{0.326}$ and $\Delta\sigma_0 = 155$ MPa, a control radius $R_C = 0.28$ mm has been proposed for welded joints.[10,29]

Atzori et al[30] showed by N-SIF and fracture mechanics analysis of welded joints with plate thicknesses between 3 and 220 mm that the stress-life behaviour of welded joints can be well approximated by both approaches in scatter bands with almost identical range. Moreover, they introduced an N-SIF threshold value $\Delta K_{1,th}^N$, which they related to the fatigue crack growth rate threshold ΔK_{th} and the El Haddad-Smith-Topper parameter a' assuming typical crack growth curve parameters and an initial crack length a_i at the fatigue limit being related to a' with the following:

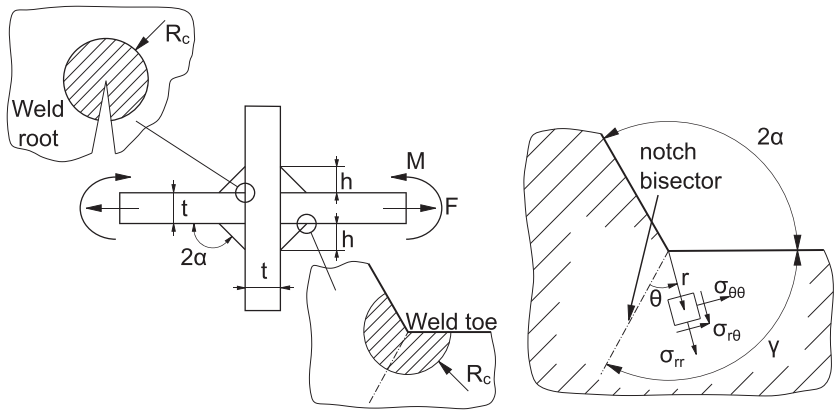

FIGURE 2 Definitions of the strain energy density method based on Lazzarin et al[27]

$$a_i = \frac{a'}{Y^2}, \tag{11}$$

where Y is the crack geometry function. The full derivation shall not be repeated here, but what is important to point out is that also for welded joints, the SED control radius R_C is directly linked to the El Haddad-Smith-Topper parameter a' and the material characteristic length L of TCD. Moreover, assuming that the SIF value necessary to nucleate a crack at a weld toe or root is equal to the threshold ΔK_{th} of the fatigue crack growth rate at 5×10^6 cycles,[30] the N-SIF threshold value $\Delta K^N_{1,th}$ is a function of ΔK_{th}.

Fischer et al[31] reanalysed the data used to derive the control radii for welded joints and suggested slightly increased radii compared to the initially proposed radii (see Table 1), since misalignment effects—especially for weld toe failures—have not been excluded while deriving the $\Delta\bar{W}$-N scatter band for welded joints. They argue that minor misalignment effects of 5% should have been considered for welded planar specimens and effects of about 10% for weld toe failures in the approach. Thus, they proposed control radii of $R_C = 0.32$ mm and $R_C = 0.325$ mm for weld toe and weld root assessment, respectively. The parameters for weld toe and root assessment are summarised in Table. 1.

Besides the slightly increased control radii, Fischer et al[32] suggested to apply a free fine mesh instead of the coarse mesh with triangular elements initially proposed by Radaj et al[33]; this results in a deviation of 0.5% from the reference value by Lazzarin and Tovo[10] for the 135° opening angle. In Figure 3, such finite element meshes for weld toe and weld root of fillet-welded joints based on a free mesh generation are presented.

TABLE 1 Calculation of R_C based on Fischer et al[31]

	Weld toe	Weld root
2α	135°	0°
e_1	0.118	0.133
λ_1	0.6736	0.5
ΔK_1^N	231 MPa mm$^{0.326}$	180 MPa mm$^{0.5}$
$\Delta\sigma_0$	1.05 × 155 MPa	1.05 × 155 MPa
R_C	0.32 mm	0.325 mm

2.3 | Application of the SED method to fatigue at high temperatures

Due to the similar effect of high temperature on material behaviour (in the absence of creep) and the lack of studies on SED-based fatigue strength assessment at sub-zero temperatures, studies will be presented that propose concepts of accounting for temperature effects in SED-based fatigue assessment. Only Viespoli et al[34] applied the SED method to fatigue strength of aluminium welded joints at sub-zero temperatures; however, no information are given whether any adjustments were made.

Recalling Equation 1, the averaged SED can either be computed numerically or for blunt notches calculated from a simplified formula according to Lazzarin and Berto[35] as follows:

$$\bar{W} = c_W F(2\alpha) \times H\left(2\alpha, \frac{R_c}{\rho}\right) \times \frac{K^2_{t,n}\sigma^2_n}{E}, \tag{12}$$

where F and H are functions describing the notch shape, c_W is a function of the stress ratio ($c_W = 1$ for $R = 0$ and $c_W = 0.5$ for $R = -1$; see Lazzarin et al[27]), $K_{t,n}$ is the stress concentration factor and σ_n is the nominal stress. This description has been successfully applied to notched and plain specimens tested at high temperatures in four recent publications.[13–16]

In Berto et al,[14] a 40CrMoV13.9 steel, typical for hot-rolling equipment, was tested and analysed in notched and unnotched states from RT up to 650°C, and fatigue test data of a Beryllium copper alloy, typical for high-

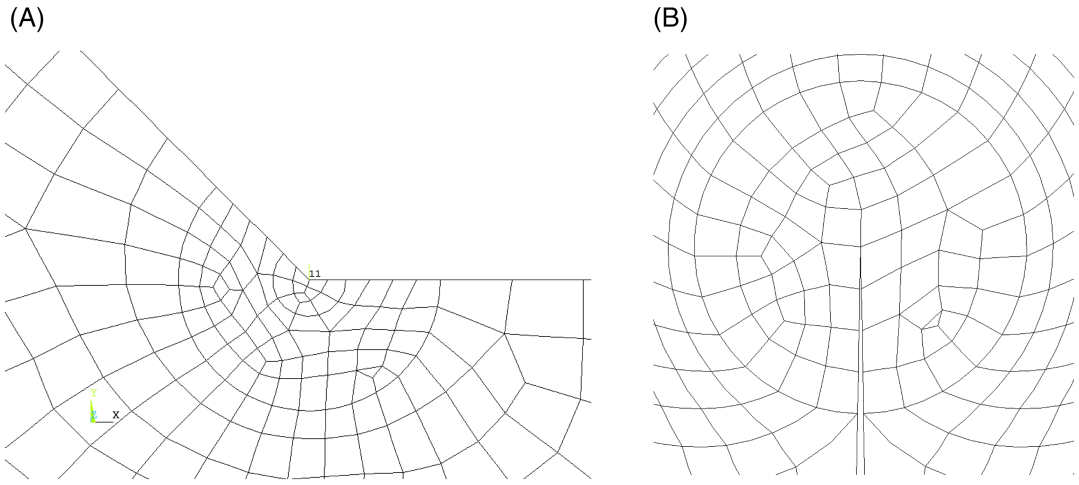

FIGURE 3 Mesh at (A) weld toe and (B) weld root of a fillet-welded joint generated by free mesh algorithm [Colour figure can be viewed at wileyonlinelibrary.com]

temperature and magnet applications, from Berto et al[13] was reassessed in terms of the SED approach. It was achieved to gather the test data for both materials, notched and unnotched states, and all temperatures together with earlier fatigue test results in one scatter band for each material. This was achieved by introducing an additional factor *Q(T)* in Equation 12, which accounts for the notch sensitivity at different temperatures. According to Berto et al,[13] the only prerequisite for using the elastic SED under Mode I loading and high temperatures is that the small-scale yielding condition is fulfilled.

Since no data were available for the El Haddad-Smith-Topper parameter a' of the Cu-Be alloy, the control radius was kept constant at $R_C = 0.6$ mm for RT and 650°C, and *Q(T)* was calculated by equating the critical SED at 2×10^6 cycles. In Gallo et al,[15] V- and semicircular notched specimens made from Titanium Grade 2 were analysed at RT and 500°C by means of the SED method. In this study, it was possible to calculate a design curve and corresponding scatter band for both notch types using $R_C = 0.3$ mm for RT and $R_C = 0.6$ mm for 500°C. A significant fatigue strength reduction of the semicircular specimens was found at 500°C; however, no synthesises of RT and high-temperature data was sought by means of a notch sensitivity factor *Q(T)*. In the most recent publication on SED-based high-temperature fatigue assessment by these authors, Gallo and Berto[16] analysed notch and plain specimens made of C45 carbon steel at 250°C, Inconel 718 at 500°C and DZ125 at 850°C reported by Louks and Susmel.[36] Using the aforementioned relation between the control radius R_C, the El Haddad-Smith-Topper parameter a' and the material characteristic length parameter L of Taylor's TCD, they were able to analyse the fatigue strength in terms of SED.

Although, in Berto et al,[14] it is only stated that *Q(T)* accounts for notch sensitivity effects it seems reasonable to assume it is directly related to the material-related support effect, which is described by the material characteristic length parameter L. Peterson[37] and Neuber[38] showed experimentally that the notch sensitivity is increasing with material strength and thus the material-related support effect is decreasing. At high temperatures, the tensile strength of materials is reduced and thereby the notch sensitivity decreased. In conclusion, it can be assumed that if the effect of temperature on the material-related support is known, described by either the El Haddad-Smith-Topper parameter a' or the material characteristic length parameter L, SED-based fatigue strength assessment can be performed for any temperature. To the author's knowledge, no such studies exist for sub-zero temperature fatigue of notch components or welded joints. Therefore, recently published fatigue test results of welded joints at sub-zero temperatures[39,40] are analysed in the following in terms of the SED.

3 | FATIGUE TEST RESULTS OF WELDED JOINTS OBTAINED AT SUB-ZERO TEMPERATURES

Braun et al[39,40] presented fatigue test results of fillet- and butt-welded joints produced from structural steels. The analysed specimens consist of butt-welded joints, a double-sided transversal stiffener and a load-carrying cruciform joint. Within this study, the results of the fillet welded joint types with weld toe and weld root failure (see Figure 4) are analysed in terms of SED since they represent the two typical notch geometries for which the

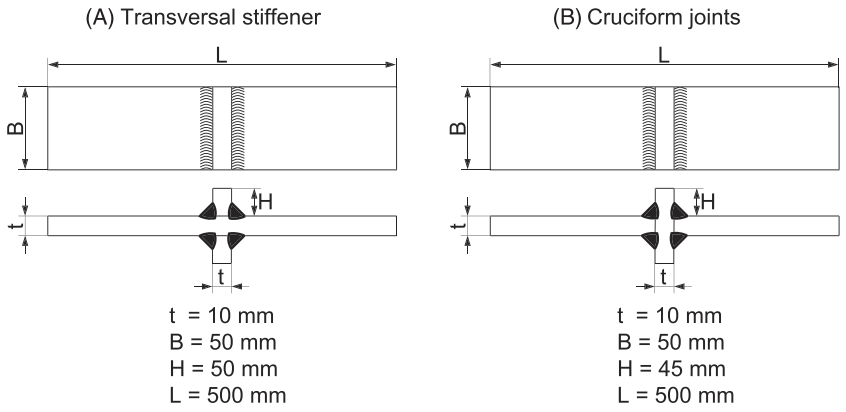

FIGURE 4 Specimen geometries of the two weld details analysed in this paper: (A) transversal stiffener and (B) cruciform joint

TABLE 2 Mechanical properties of steels used[42]

Steel	T [°C]	σ_{UTS} [MPa]	e_f [%]
S235J2+N	20	453.5	30.6
	−20	469.3	25.6
	50	485.9	23.3
S500G1+M	20	597.4	19.0
	−20	643.8	18.6
	−50	644.5	15.3

SED method was originally developed (i.e., $2\alpha = 135°$ and $2\alpha = 0°$ at weld toe and root, respectively). The butt-welded joints have not been included due to material strength related differences in fatigue strength (difference in fatigue strength of more than 10% between S235 and S500 specimens) and the missing concepts to model butt joints with large weld toe radii (here up to 3 mm, see Braun et al[40]). The assumption of a V-type notch is thus not feasible, see Berto and Lazzarin.[22]

FIGURE 5 Cruciform joint specimen before a fatigue test, taken from Braun et al[39] [Colour figure can be viewed at wileyonlinelibrary.com]

Tests results are presented in the range from RT, that is, 20°C, down to −50°C. This temperature range seems representative for a ship travelling through Arctic regions year round.[41] The specimens were produced from two structural steels: a normalised steel (S235J2+N) and a fine-grained thermomechanically rolled steel (S500G1+M) with the mechanical properties listed in Table 2. All specimens were welded by means of flux-cored arc welding process, see Braun et al[39] for further details. Before the test, the misalignment and local weld geometry of every specimen were measured based on the curvature method (see other studies[43,44]). Thus, the actual throat thickness of each cruciform specimens has been used to calculate the nominal stress acting in the fillet weld.

Fatigue testing was carried out under axial loading, with a stress ratio $R = 0$, in a temperature chamber cooled by vapourised nitrogen, see Figure 5. The analysed dataset consists of 143 fatigue test results in total. Figure 6 presents the results in addition with the *S-N* curve for 50% survival probability together with results of recent tests of cruciform joints and transversal stiffener. In all subfigures, the corresponding fatigue design curve (FAT) according to the International Institute of Welding (IIW) recommendations[45] is included.

All test series have been evaluated using the recommended slope $k = 3$ for welded joints according to IIW recommendations.[45] Moreover, the specimens showed generally small misalignment levels (below the level that requires correction of nominal stress results, see Braun et al[3]).

The results in terms of SED are presented in Figure 7. All test series of the transversal stiffener series are indicated with a "WT" (weld toe failure) and cruciform joints with weld root failure with a "WR." Moreover, filled symbols are used for S500 steel and empty for S235 steel. The colour scheme for the temperature range is black (RT), red (−20°C) and blue (−50°C).

In order to highlight the outcome of an assessment with material parameters derived at RT, the proposed

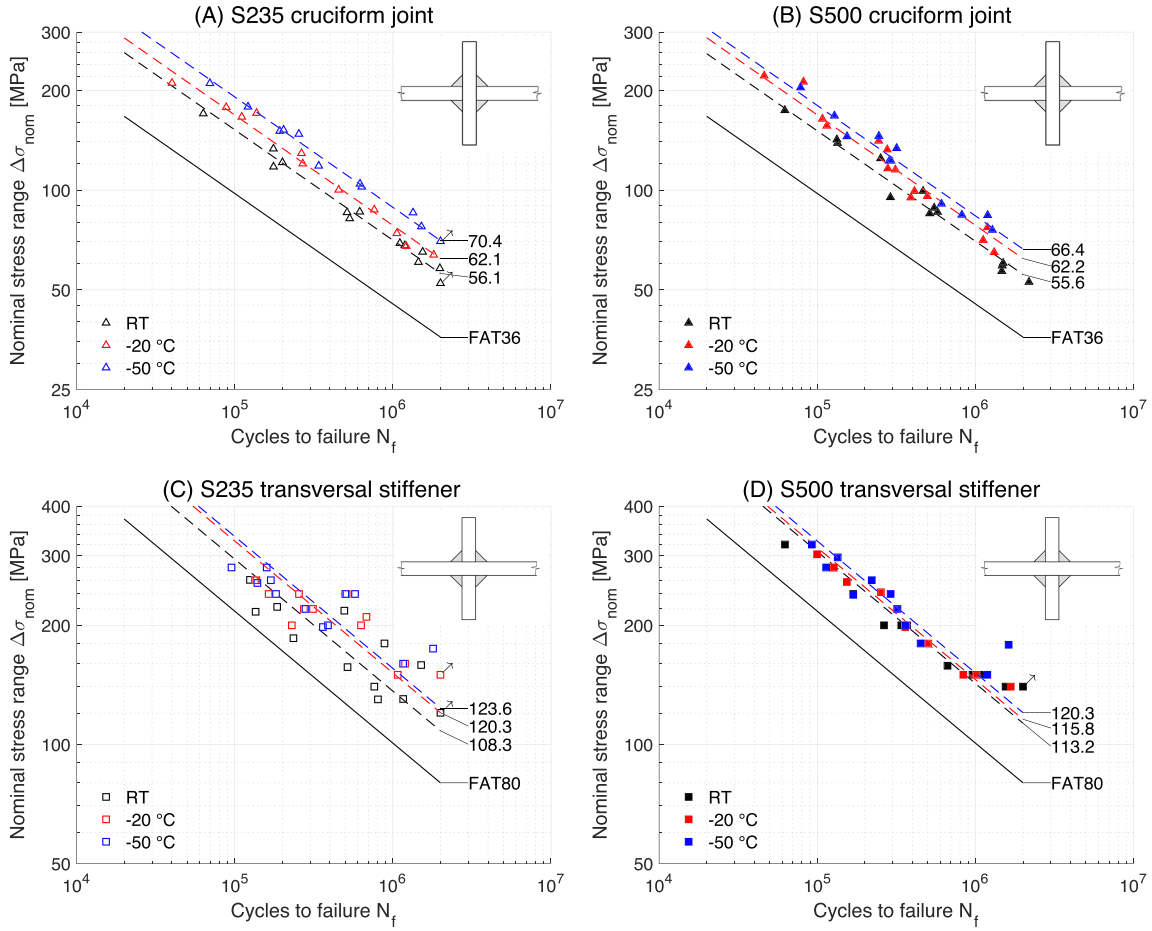

FIGURE 6 Results of the fatigue tests at different temperatures for the two different steels and joint types, data from Braun et al[39] [Colour figure can be viewed at wileyonlinelibrary.com]

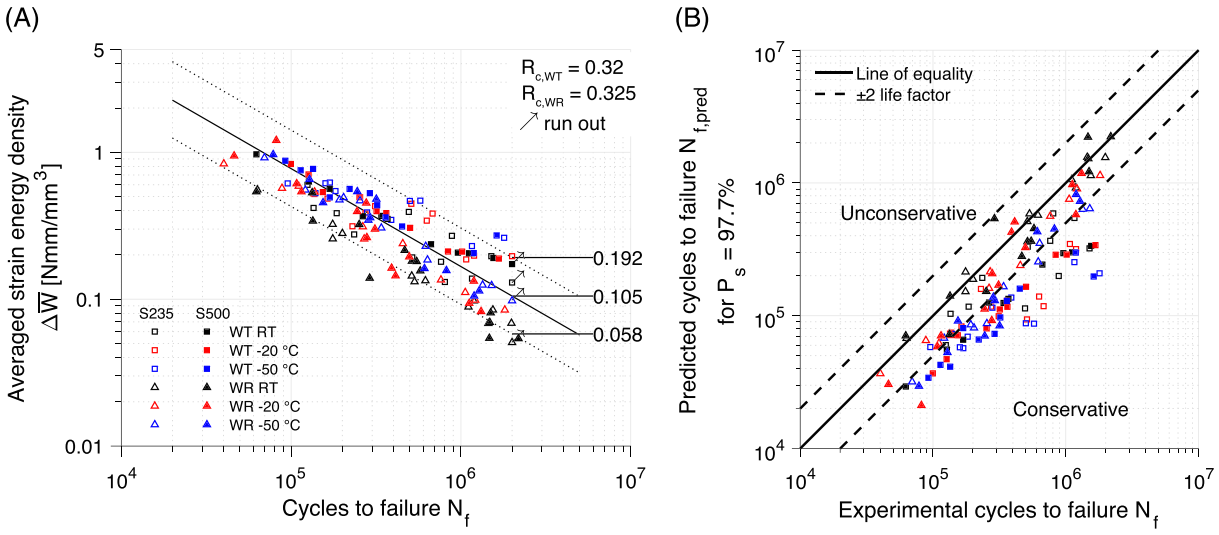

FIGURE 7 (A) Results for sub-zero temperatures with room temperature control radii for weld toe and root failure ($R_{c,WT}$ = 0.32 mm and $R_{c,WR}$ = 0.325 mm), and (B) comparison of experimental and predicted cycles to failure [Colour figure can be viewed at wileyonlinelibrary.com]

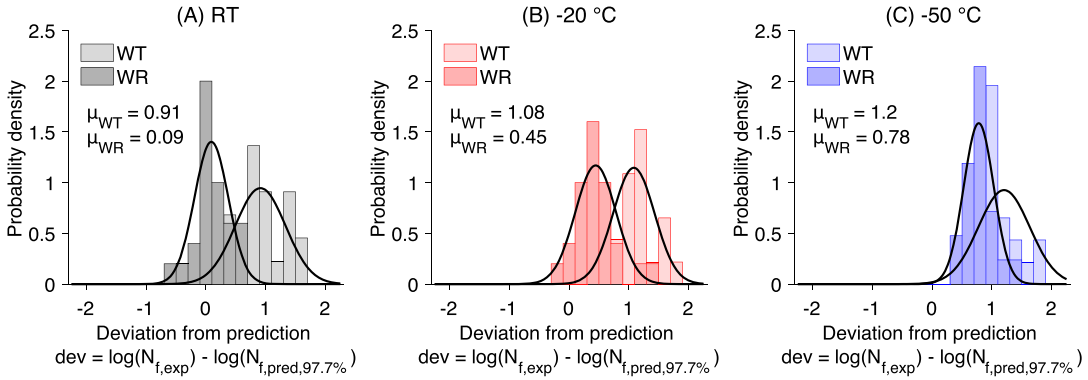

FIGURE 8 Deviation between experimental and predicted cycles at room temperature (RT), −20°C and −50°C [Colour figure can be viewed at wileyonlinelibrary.com]

control radii by Fischer et al[31] and a Young's modulus of 206 GPa are applied. Moreover, a free mesh generation inside the control radius is applied (see Figure 3).

Due to the small variation of throat thickness between the test specimens, the median weld throat thickness is used in the FE models of the cruciform joints (i.e., $a = 5.71$ mm and $a = 5.85$ mm for S235 and S500 cruciform joints, respectively); however, the throat thickness of each specimen is used to calculate the actual nominal stress. Moreover, secondary bending effects due to misalignment are considered in a simplified way as an increased nominal stress, which is thought to be conservative.[3,43] For this purpose, the standard formulas given in international standard and guidelines are applied, see other studies.[45,46]

First of all, the fatigue data of most test series fit nicely into the proposed scatter band for welded joints[47]; and, as expected, the fatigue strength of the tests at sub-zero temperatures are closer to the upper limit of the scatter band. Furthermore, a slightly higher fatigue strength is observed for transversal stiffeners compared to cruciform joints. In Figure 8, the distribution of the logarithmic deviation between the experimental $N_{f,exp}$ and the predicted cycles to failure $N_{f,pred,97.7\%}$ based on the lower bound of the scatter band are presented, which are calculated as follows:

$$\mathrm{dev} = \log N_{f,exp} - \log N_{f,pred,97.7\%}. \quad (13)$$

Due to the different radii used, the results are plotted separately for the two failure locations (weld toe and root). Moreover, μ_{WT} and μ_{WR} refer to the mean deviation for specimens showing weld toe and weld root failure. In general, the test results at sub-zero temperatures could be assessed with the scatter band proposed derived from tests at RT; however, this would lead to unnecessary conservatism due to the increasing deviation between design curve and fatigue strength at sub-zero temperatures. In the following section, a concept of including temperature effects in fatigue assessment of welded joints without the need for modification factors or new scatter bands is presented.

4 | EXTENSION OF THE SED METHOD TO ASSESS THE FATIGUE STRENGTH OF WELDED JOINTS TESTED AT SUB-ZERO TEMPERATURES

4.1 | Synthesis of sub-zero temperatures fatigue test results

First of all, as mentioned in Section 2.1, the expected changes of material support effect with temperature are linked to the size of the control radius R_c via the material characteristic length parameter L or the El Haddad-Smith-Topper parameter a'. At low temperatures, the material strength is known to increase.[48,49] Thus, a decrease of L and a' is expected for sub-zero temperatures; however, measuring the material support effect by either parameter requires a large number of specimens. Consequently, the change in material support effect is here derived by finding the control radius R_c at sub-zero temperatures that fits the test data best, that is, leading to the same mean deviation from the proposed scatter band for all test temperatures based on Equation 13.

Berto et al[14] have shown that fatigue test data in the range from RT to 500°C can be summarised in one scatter band using one control radius and the proposed notch sensitivity function. For 650°C, a separate scatter band with different slope was proposed due to the change in underlying fracture behaviour. Thus, it can be assumed

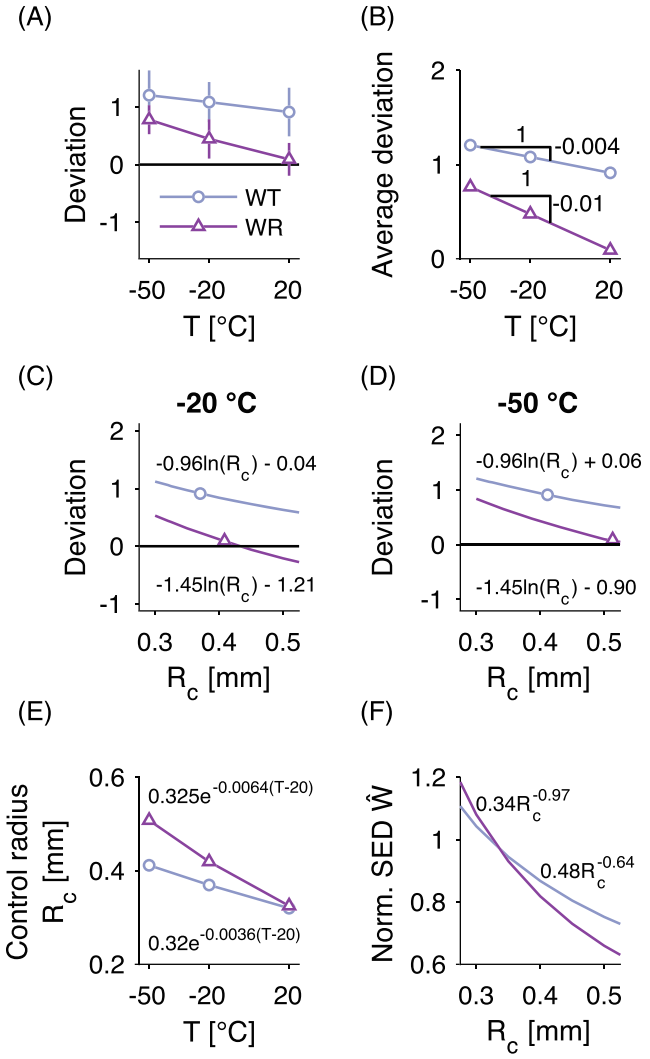

FIGURE 9 (A) Deviation between experimental and predicted cycles to failure, (B) average deviation relative to RT, deviation as a function of control radius R_c for (C) −20°C and (D) −50°C, (E) control radii as a function of temperature, and (F) normalised elastic strain energy density $\hat{W}$ as a function of the control radii [Colour figure can be viewed at wileyonlinelibrary.com]

that the same scatter band can be applied also for sub-zero temperatures as long as the underlying fracture behaviour is unchanged and the small-scale yielding condition is fulfilled. For high-cycle fatigue and sub-zero temperatures above the ductile-brittle transition temperature, those assumptions are fulfilled.

Beside the fatigue strength, also the Young's modulus is affected by temperature effects. From Equation 1, it becomes apparent that the change in Young's modulus with temperature is directly accounted for by the elastic SED. Here, the Young's modulus is assumed to change 10 GPa for every 100°C of temperature change (cf. other studies[49–51]). This change agrees with data reported in standards like BS7910[46] for high temperature below the creep limit; however, a smaller increase in Young's modulus is assumed in BS7910[46] for sub-zero temperatures (see Braun et al[39] for further discussion). In this paper, a change of Young's modulus 10 GPa for every 100°C of temperature change is assumed for sub-zero temperatures (i.e., 202 GPa at −20°C and 199 GPa at −50°C).

From Figure 8, a clear trend towards a higher deviation of the experimental from the predicted fatigue strength (based on the proposed scatter band for RT) is unambiguous. In order to highlight the change in deviation with decreasing temperature, the mean and standard deviation (indicated by vertical lines around the mean value) of the logarithmic deviation is presented in Figure 9A for the two specimen types and corresponding failure locations.

Interestingly, an almost linear increase is observed for both specimen types with decreasing temperature. Thus, in Figure 9B, the average deviation relative to RT is presented including the change in temperature per degree Celsius (illustrated by the slope triangle).

In the next step, the control radius R_c at sub-zero temperatures—that fits the test data best—is derived by assessing the mean deviation (dev) that results from varying the control radii R_c for WT and WR. The logarithmic relation between both parameters is presented in Figure 9C,D for −20°C and −50°C, respectively, and both failure locations. From the equations besides the curves, the control radius R_c that yields the average deviation at −20°C and −50°C according to Figure 9B is calculated. The resulting control radii, being for the weld toe $R_c = 0.37$ mm at −20°C and 0.41 mm at −50°C as well as $R_c = 0.41$ mm at −20°C and 0.51 mm at −50°C for the weld root, are marked on the graphs in Figure 9C,D. Subsequently, the so-derived control radii are plotted against test temperature in Figure 9E.

From the estimated control radii, it is possible to derive a general recommendation for control radii to be applied for SED-based fatigue assessment of engineering structures subjected to sub-zero temperatures as follows:

$$\text{Weld toe failure } (2\alpha = 135^\circ): R_{c,\mathrm{WT}} = 0.32e^{-0.0036(T-20)}; \text{for } T \text{ in}^\circ\text{C}, \quad (14)$$

$$\text{Weld root failure } (2\alpha = 0^\circ): R_{c,\mathrm{WR}} = 0.325e^{-0.0064(T-20)}; \text{for } T \text{ in}^\circ\text{C}. \quad (15)$$

Since the operating temperature and thus material temperature of engineering structures like ships and offshore structures exposed to arctic conditions can vary a lot, it seems infeasible to adjust the control radii for lots of different temperatures. Thus, a temperature

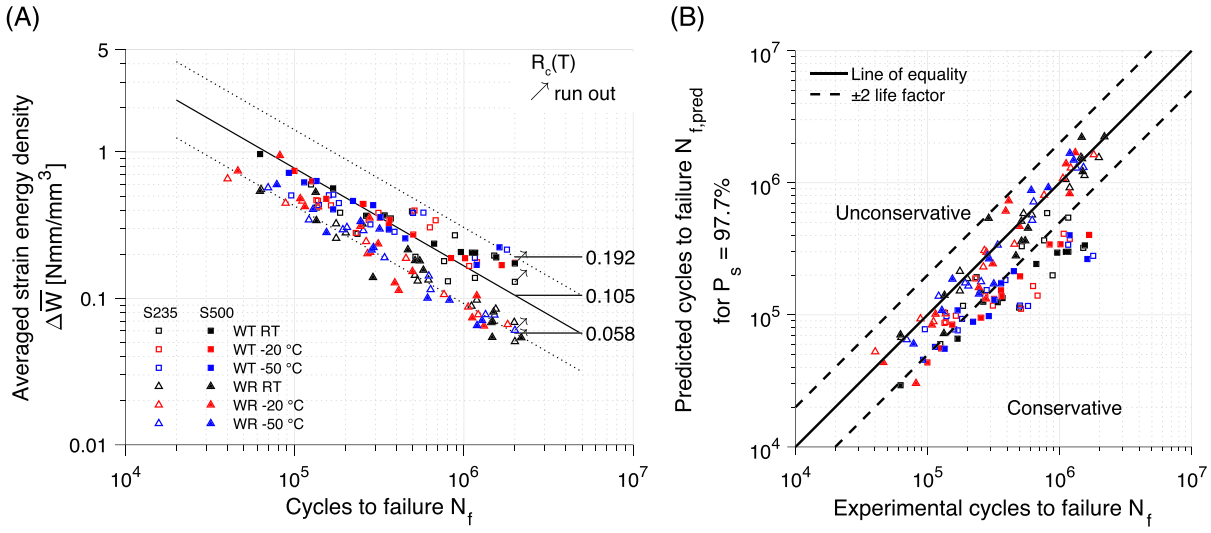

FIGURE 10 Results for sub-zero temperatures with control radius R_c adjusted to sub-zero temperatures [Colour figure can be viewed at wileyonlinelibrary.com]

modification formula $M(T)$ for the SED—similar to the notch shape functions F and H of Equation 12—shall be introduced. In Figure 9F, the relation between normalised elastic SED $\hat{W}$ and the control radius (i.e,. the percentage change of W with respect to R_c) is presented for the weld toe and weld root. By inserting Equation 14 and Equation 15 in the corresponding equation given in Figure 9F, the following temperature modification function is derived for weld toe and weld root failure:

$$M(T) = \begin{cases} \left(e^{-0.0036\,(T-20)}\right)^{-0.64} & \text{if } 2\alpha = 135° \\ \left(e^{-0.0064\,(T-20)}\right)^{-0.97} & \text{if } 2\alpha = 0° \end{cases} ;T \text{ in}^\circ\text{C}. \tag{16}$$

Applying the aforementioned calculated control radii for weld toe and root and −20°C and −50°C, it is possible to assess the fatigue test results obtained at sub-zero temperatures in the same scatter band proposed for RT, see

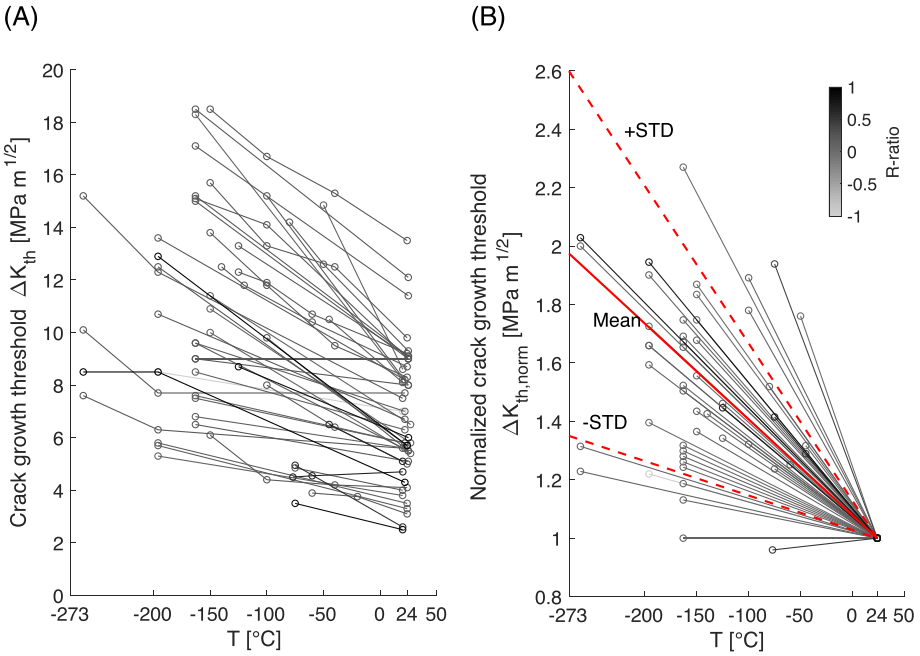

FIGURE 11 (A) Sub-zero temperatures ΔK_{th} data extracted from literature and (B) normalised average ΔK_{th} change at sub-zero temperatures from 50 datasets reported in literature[52–75] [Colour figure can be viewed at wileyonlinelibrary.com]

Figure 10. Compared with Figure 7, all transversal stiffener specimens are now inside the proposed scatter band. The results of the cruciform joints are scattered around the lower end of the proposed scatter band (i.e., around the $\Delta\bar{W}-N$ curve for 97.7% survival probability). The same result was observed by Fischer et al[31] for the same specimen type and specimen thickness. Nonetheless, the SED method is much better suited to capture temperature effects on fatigue strength due to the link between the size of the control radius R_c and the material support effect than stress-based fatigue assessment methods. Applying stress-based concepts, changes in fatigue strength at sub-zero temperatures can only be covered by modification factors, see Braun et al.[3]

By applying the aforementioned concept, the mean deviation of the fatigue life prediction of the transversal stiffener to RT results is reduced from 18.7% at −20°C and 31.9% at −50°C to 1.1% and 0%, respectively.

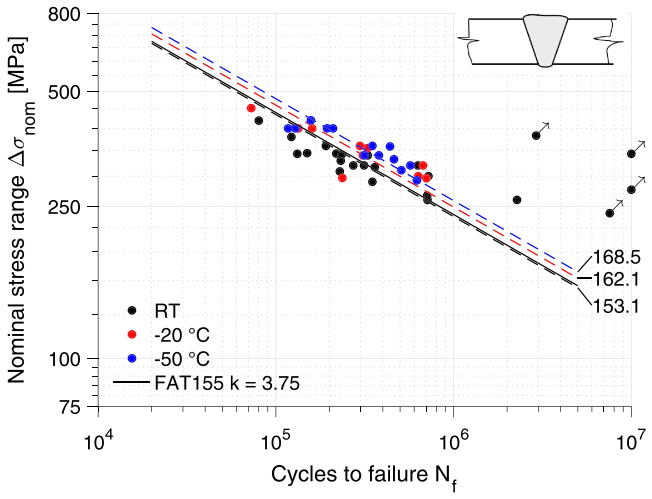

FIGURE 12 *S–N* results of S500 butt-welded joints assessed with a fixed slope exponent of $k = 3.75$, data from Braun et al[40] [Colour figure can be viewed at wileyonlinelibrary.com]

5 | ASSESSMENT OF THE RESULTS USING DATA OF MATERIAL FATIGUE

In order to evaluate the feasibility of the adjusted control radii R_c for sub-zero temperatures, the components from which R_c for welded joints was originally derived for RT are evaluated at sub-zero temperatures. Recalling Equation 10, R_c is derived from ΔK_1^N and fatigue limit $\Delta\sigma_0$ of butt welds without a notch. ΔK_1^N at sub-zero temperatures can be estimated based on literature data; however, there are no data available for $\Delta\sigma_0$ at sub-zero temperatures. Thus, a comparison with the initially presented test data on butt-welded joints (that show a similar fatigue strength as flush-ground butt welds) will be performed.

In order to estimate the change of ΔK_1^N with temperature, it is possible to make use of the relation between the threshold of fatigue crack growth rate ΔK_{th} and the N-SIF threshold value $\Delta K_{1,th}^N$. Assuming a linear relation between both quantities at $5\text{x}10^6$ cycles (see Atzori et al[30]), the change of N-SIF threshold value $\Delta K_{1,th}^N$ can be estimated from the change of fatigue crack growth rate threshold ΔK_{th} at sub-zero temperatures.

In total, 52 datasets were extracted from literature that report fatigue crack growth rate threshold ΔK_{th} at sub-zero temperatures.[52–75] The results are presented in Figure 11A. First of all, the data is analysed regarding different influencing factors within the datasets, but no particular peculiarities are found for stress ratio, material (ferritic/austenitic), base material or welded material. Seven datasets were found for stress ratios above $R = 0.1$ and one for $R = -1$. The remaining data were measured for ratios between $R = 0$ and $R = 0.1$. Two datasets have been rejected since the change in threshold value seemed unreasonably high compared with all other datasets.

Since a lot of studies focused on the determination of the fatigue transition temperature to brittle material behaviour, only data points, which are clearly above the transition temperature, were considered for the assessment. Only one dataset is found with a decreasing average threshold value at low temperatures; however, the value is assumed to be above the transition temperature based on the other reported results in the same study. Unsurprisingly, the higher the initial threshold value, the higher the increase at low temperatures; however, in order to use the data to estimate the median increase $k_{\Delta K_{th,norm}}$ in fatigue crack growth rate threshold ΔK_{th} at sub-zero temperatures, the average slope of each dataset was normalised by the threshold at RT. The calculated normalised mean slope is $k_{\Delta K_{th,norm}} = -0.0033$ MPa√m/°C (red line in Figure 11B) with a standard deviation (STD) of 0.0021 MPa√m/°C (leading to the dashed red lines).

The average reported RT was 23.9°C with a standard deviation of 2.2°C. Due to the minor deviation in reported RT and for presentation purpose, the normalised fatigue crack growth rate threshold $\Delta K_{th,norm}$ with temperature is presented in Figure 11B by setting the RT to 23.9°C. All datasets are presented in the actual tested temperature range of each study.

Based on the linear relation between ΔK_{th} and ΔK_1^N, an increase of ΔK_1^N of about 12% at −20°C and 21% at −50°C is estimated compared with an RT of 20°C (room test temperature of this study); this agrees well with the change in nominal fatigue strength of the cruciform joints at those two temperatures. Due to the sharp notch

radii and the zero opening angle at the weld root, the fatigue life of cruciform joints failing from the weld root is almost entirely driven by crack propagation. Consequently, a similar change in threshold value and nominal fatigue strength seems reasonable.

Based on the change of ΔK_1^N, the required change in plain-specimen fatigue strength $\Delta\sigma_0$ at sub-zero temperature to yield the calculated control radii R_c at sub-zero temperatures can be estimated by rearranging Equation 10.

$$\Delta\sigma_0 = \frac{\sqrt{2e_1} \times \Delta K_1^N}{{R_C}^{1-\lambda_1}}. \tag{17}$$

Inserting the calculated control radii R_c and increasing ΔK_1^N by 12% and 21% for −20°C and −50°C, respectively, a changed strength of plain specimen fatigue (ground flush butt joints) to about 158 and 165 MPa is calculated for weld toe failure at −20°C and −50°C, respectively. For weld root failure, an increase to about 162 MPa is estimated at −20°C and a slight decrease to 157 MPa for −50°C. Given the uncertainty in calculated mean slope of the fatigue crack growth rate threshold at sub-zero temperatures, the level of increase seems reasonable.

As initially mentioned, fatigue testing of plain butt-welded specimens would be a complex and costly task (see other works[31,76]). Instead, data of high quality S500 butt-welded joints are used as a reference here from Braun et al.[40] They have been tested under the same conditions presented in Section 3. Due to the large weld toe radii up to 3 mm, the fatigue strength exceeds the reference fatigue strength for butt-welded joints according to international standards by far, see Braun et al.[40] The actual fatigue strength and natural slope are indeed quite close to the fatigue strength of ground-flush butt-welded joints in literature (155 MPa for $N_f = 5 \times 10^6$ and 50% survival probability). The, fatigue test results of the S500 butt-welded joints are thus re-evaluated using a fixed slope exponent $k = 3.75$ (often used to asses ground-flush butt-welded joints[31]). The results are presented in Figure 12. For comparison, the fatigue strength at five million cycles is presented along with the FAT155 curve. The results are remarkably close to the estimated plain specimen fatigue strength by Equation 14 for weld toe failure at −20°C and −50°C and weld root failure at −20°C. Only the results for weld root failure and −50°C show a different trend with lower plain specimen fatigue strength at −50°C.

The estimate of a smaller increase of plain specimen fatigue strength, based on the proposed control radii and literature data of threshold of fatigue crack growth rate ΔK_{th} for sub-zero temperatures, is thus confirmed.

6 | DISCUSSION

In this study, a concept is presented to derive control radii R_c for sub-zero temperatures fatigue assessment of welded steel joints. Due to the lack of studies concerning low temperatures, the idea is based on previous studies of Berto et al[13–16] for high-temperature fatigue of notched components. In order to evaluate the derived control radii R_c, the relation between R_c, the N-SIF ΔK_1^N and fatigue limit $\Delta\sigma_0$ of butt welds without a notch is applied. Due to missing data for both quantities, the relation between ΔK_1^N and stress-intensity factor threshold for long cracks ΔK_{th} as well as presented test data on butt-welded joints (that show a similar fatigue strength as flush-ground butt welds) is used for evaluation.

Judging the seemingly larger increase in stress-intensity factor threshold for long cracks ΔK_{th} compared with the expected smaller relative change in plain specimen fatigue strength $\Delta\sigma_0$, an increase in the El Haddad-Smith-Topper parameter a' or material characteristic length L at sub-zero temperatures is expected. Verifying the observed trend by testing for the actual material characteristic length of welded joints seems practically infeasible, since it would require tests to be performed at the exact same load ratio according to Louks and Susmel,[36] which would mean that the local stress ratio of each specimen would have to be accounted for. It is well known that the local stress ratio at the crack initiation location may vary considerably from the applied nominal stress ratio, due to welding residual stresses, local stress concentration and misalignment effects; however, further tests on flush-ground butt-welded specimens are one possibility to support the observed trend. Interestingly, a similar trend of increased material characteristic length L was observed using the stress averaging approach.[8]

Based on the presented concept, it is possible to assess the fatigue strength of specimens failing from weld toe or weld root by means of the originally proposed $\Delta\bar{W}-N$ scatter band for welded joints. Similar concepts have successfully been introduced by Berto et al[14] for notched and unnotched 40CrMoV13.9 steel specimens tested at high temperatures; however, instead of introducing an empirical temperature sensitivity function $Q(T)$, synthesis of the fatigue test data at different temperatures is achieved by finding the control radii R_c that fit the data best (i.e., leading to the same deviation from the design curve as for RT test data). Moreover, temperature effects on Young's modulus and changes of material support effect via changed control radii with temperature are directly accounted for by this procedure; this agrees with previous findings of Gallo and Berto[16] for high-temperature fatigue of notched components. Thus, temperature effects

on fatigue strength are accounted for on a sound physical basis, and no modification factors (as for stress-based fatigue assessment methods) are required.

7 | CONCLUSIONS

This study investigated the possibility of extending the SED method for fatigue assessment to welded joints exposed to sub-zero temperatures. For this purpose, fatigue test results of fillet-welded steel joints with weld toe and weld root failure by Braun et al[39] in the range of 20°C down to −50°C were used to derive control radii suitable for the application of the SED method at sub-zero temperatures. The results are evaluated based on the formula that is used to derive the control radii of welded joints. For this purpose, fatigue crack growth threshold test results found in literature and estimates of the plain specimen fatigue strength of ground-flush butt-welded joints at sub-zero temperatures are applied. From the estimates of the control radii at sub-zero temperatures, temperature modification functions for the SED are derived for design purposes. From the investigation, the following conclusions are drawn:

- It is possible to gather the fatigue strength of welded joints in the same scatter band of the SED method for welded joints—that was initially proposed for fatigue at RT—if changes of material support effect and Young's modulus at sub-zero temperatures are accounted for by changing the control radii.
- Suitable control radii at sub-zero temperature can be derived by enforcing the deviation between design curves to be the same at RT and sub-zero temperatures.
- Thus, the introduction of modification factors for temperatures different than RT can be avoided—as it is required for stress-based concepts. Nonetheless, temperature modification functions for the SED are derived to ease fatigue design by means of the SED method.
- The proposed concept for sub-zero temperatures and the obtained SED control radii are assessed based on the parameters the control radii are derived from. Using data of material fatigue at sub-zero temperature, that is, of stress intensity factor threshold ΔK_{th} at sub-zero temperatures found in literature and test results of butt-welded joints with similar fatigue strength as flush ground butt-welded joints, a good agreement with the proposed concept is achieved.

ACKNOWLEDGEMENTS

The work was funded by the German Federal Ministry for Economic Affairs and Energy (Bundesministerium für Wirtschaft und Energie BMWi) in the framework of MarTERA ERA-NET Cofound scheme (MarTERA – FATICE (03SX465B)). Open access funding enabled and organized by Projekt DEAL.

AUTHOR CONTRIBUTIONS

Writing: Moritz Braun. Model development and investigation: Moritz Braun and Claas Fischer. Conceptualization and methodology: all authors. All authors have read and agreed to the published version of the manuscript.

NOMENCLATURE

a'	El Haddad-Smith-Topper parameter
a_i	initial crack length at the fatigue limit
B, H, L, t	specimen's width, stiffener height, length and thickness
c_W	SED stress ratio function
dev	logarithmic deviation between the experimental and the predicted cycles to failure
e_f	elongation at fracture
e_1, e_2	SED stress-strain field correction factors
F, H	SED notch shape functions
k	slope exponent of the stress-life curve
$K_{t,n}$	stress concentration factor
K_1 and K_2	N-SIF for modes I and II
L	material characteristic length
$M(T)$	temperature modification formula
N_f, $N_{f,exp}$, $N_{f,pred,97.7\%}$	number of cycles to failure, experimental number of cycles to failure and number of cycles to failure for 97.7% survival probability
r_0	distance between the V-notch tip and the origin of the local coordinate system
R	stress ratio between lower and upper stress
$Q(T)$	notch sensitivity function
R_c, $R_{c,WT}$, $R_{c,WR}$	control radius, control radius at weld toe and at weld root
T	temperature
$\bar{W}, \Delta\bar{W}, \hat{W}$	averaged SED, SED range and normalised SED
Y	crack geometry function
2α, γ	notch opening angle and bisector
$\Delta K_{th}, \Delta K^N_{1,th}$	fatigue crack growth threshold for long cracks and Mode I N-SIF threshold value
ΔK^N_1	Mode I N-SIF fatigue strength for notched component
$\Delta K_{th,norm}$, $k_{\Delta K_{th,norm}}$	normalised fatigue crack growth rate threshold of ΔK_{th} vs. T data and mean slope of $\Delta K_{th,norm}$
$\Delta\sigma_0$	fatigue limit of smooth base material specimen

λ_1 and λ_2	eigenvalues of the Williams' stress field solution for the N-SIF K_1 and K_2 for modes I and II
μ_{WT}, μ_{WR}	mean deviation for specimens showing weld toe and weld root failure
ν	Poisson's ratio
ρ	real notch radius
σ_n, $\Delta\sigma_n$	nominal stress and nominal stress range
σ_{rr}, $\sigma_{r\Theta}$ and $\sigma_{\Theta\Theta}$	stress components in polar coordinates (r, Θ)
σ_{UTS}, σ_{YS}	ultimate tensile and yield strength

ORCID

Moritz Braun https://orcid.org/0000-0001-9266-1698
Sören Ehlers https://orcid.org/0000-0001-5698-9354

REFERENCES

1. Milaković A-S, Gunnarsson B, Balmasov S, et al. Current status and future operational models for transit shipping along the Northern Sea Route. *Mar Policy*. 2018;94:53-60.
2. von Bock und Polach RUF, Klein M, Kubiczek J, Kellner L, Braun M, Herrnring H. State of the art and knowledge gaps on modelling structures in cold regions. ASME 2019 38th International Conference on Ocean, Offshore and Arctic Engineering June 9–14, 2019; Glasgow, Scotland.
3. Braun M, Milaković A-S, Renken F, Fricke W, Ehlers S. Application of local approaches to the assessment of fatigue test results obtained for welded joints at sub-zero temperatures. *Int J Fatig*. 2020;138:105672.
4. Hobbacher AF. Comparison of fatigue verification procedures at a thick-walled welded component. *Weld World*. 2017;61(4):801-818.
5. Braun M, Grimm J-H, Milaković A-S, Hoffmeister H, Canaletti A, Ehlers S, Fricke W. Bewertung der Schwingfestigkeit ausgeschliffener Schweißnähte aus hochfesten Stählen und Vergleich mit gekerbten Grundmaterialproben. 19. Hamburg, Germany: Tagung Schweißen in der maritimen Technik und im Ingenieurbau; 2019.
6. Baumgartner J, Yıldırım HC, Barsoum Z. Fatigue strength assessment of TIG-dressed welded steel joints by local approaches. *Int J Fatig*. 2019;126:72-78.
7. Yildirim HC, Marquis GB, Barsoum Z. Fatigue assessment of high frequency mechanical impact (HFMI)-improved fillet welds by local approaches. *Int J Fatig*. 2013;52:57-67.
8. Braun M, Milaković A-S, Ehlers S. Fatigue assessment of welded joints at sub-zero temperatures using the stress averaging approach. International Conference on Ships and Offshore Structures ICSOS 2020; 1–4 September, 2020; Glasgov, UK.
9. Williams ML. Stress distribution at the base of a stationary crack. *J Appl Mech*. 1956;24(1):109-114.
10. Lazzarin P, Tovo R. A notch intensity factor approach to the stress analysis of welds. *Fatigue Fract Eng Mater Struct*. 1998;21(9):1089-1103.
11. Gillemot LF. Criterion of crack initiation and spreading. *Eng Fract Mech*. 1976;8(1):239-253.
12. Sih GC. Strain energy density factor applied to mixed mode crack problems. *Int J Fract*. 1974;10(3):305-321.
13. Berto F, Lazzarin P, Gallo P. High-temperature fatigue strength of a copper–cobalt–beryllium alloy. *J Strain Anal Eng Des*. 2013;49(4):244-256.
14. Berto F, Gallo P, Lazzarin P. High temperature fatigue tests of un-notched and notched specimens made of 40CrMoV13.9 steel. *Mater Des*. 2014;63:609-619.
15. Gallo P, Berto F, Lazzarin P. High temperature fatigue tests of notched specimens made of titanium grade 2. *Theor Appl Fract Mech*. 2015;76:27-34.
16. Gallo P, Berto F. Advanced materials for applications at high temperature: fatigue assessment by means of local strain energy density. *Adv Eng Mater*. 2016;18(12):2010-2017.
17. Lazzarin P, Berto F, Zappalorto M. Rapid calculations of notch stress intensity factors based on averaged strain energy density from coarse meshes: theoretical bases and applications. *Int J Fatig*. 2010;32(10):1559-1567.
18. Kitagawa H, Takahashi S. Applicability of fracture mechanics to very small cracks or the cracks in the early stage. Second International Conference on Mechanical Behavior of Materials. ASM, Metals Park, Ohio; 1976; 627–631.
19. Atzori B, Lazzarin P. Notch sensitivity and defect sensitivity under fatigue loading: two sides of the same medal. *Int J Fract*. 2001;107(1):1-8.
20. Lazzarin P, Berto F, Gomez FJ, Zappalorto M. Some advantages derived from the use of the strain energy density over a control volume in fatigue strength assessments of welded joints. *Int J Fatig*. 2008;30(8):1345-1357.
21. Lazzarin P, Zambardi R. A finite-volume-energy based approach to predict the static and fatigue behavior of components with sharp V-shaped notches. *Int J Fract*. 2001;112(3):275-298.
22. Berto F, Lazzarin P. A review of the volume-based strain energy density approach applied to V-notches and welded structures. *Theor Appl Fract Mech*. 2009;52(3):183-194.
23. El Haddad M, Topper T, Smith K. Prediction of non-propagating cracks. *Eng Fract Mech*. 1979;11(3):573-584.
24. Taylor D. *The Theory of Critical Distances: A New Perspective in Fracture Mechanics*. Oxford, UK: Elsevier; 2007.
25. Braun M, Müller AM, Milaković A-S, Fricke W, Ehlers S. Requirements for stress gradient-based fatigue assessment of notched structures according to theory of critical distance. *Fatigue Fract Eng M*. 2020;43(7):1541-1554.
26. Radaj D, Vormwald M. *Ermüdungsfestigkeit: Grundlagen für Ingenieure*. 3rd ed. Berlin Heidelberg: Springer; 2007.
27. Lazzarin P, Livieri P, Berto F, Zappalorto M. Local strain energy density and fatigue strength of welded joints under uniaxial and multiaxial loading. *Eng Fract Mech*. 2008;75(7):1875-1889.
28. Livieri P, Lazzarin P. Fatigue strength of steel and aluminium welded joints based on generalised stress intensity factors and local strain energy values. *Int J Fract*. 2005;133(3):247-276.
29. Atzori B, Dattoma V. A comparison of fatigue behaviour of welded joints in steel and aluminium alloys. *International Institute of Welding IIW-Doc*. XIII-1089-83; 1983.
30. Atzori B, Lazzarin P, Meneghetti G. Fatigue strength assessment of welded joints: from the integration of Paris' law to a synthesis based on the notch stress intensity factors of the uncracked geometries. *Eng Fract Mech*. 2008;75(3–4):364-378.

31. Fischer C, Fricke W, Rizzo CM. Review of the fatigue strength of welded joints based on the notch stress intensity factor and SED approaches. *Int J Fatig*. 2016;84:59-66.
32. Fischer C, Fricke W, Rizzo CM. Experiences and recommendations for numerical analyses of notch stress intensity factor and averaged strain energy density. *Eng Fract Mech*. 2016;165:98-113.
33. Radaj D, Berto F, Lazzarin P. Local fatigue strength parameters for welded joints based on strain energy density with inclusion of small-size notches. *Eng Fract Mech*. 2009;76(8):1109-1130.
34. Viespoli LM, Leonardi A, Cianetti F, Nyhus B, Alvaro A, Berto F. Low-temperature fatigue life properties of aluminum butt weldments by the means of the local strain energy density approach. *Mater Des Process Comm*. 2019;1(1):e30.
35. Lazzarin P, Berto F. Some expressions for the strain energy in a finite volume surrounding the root of blunt V-notches. *Int J Fract*. 2005;135(1–4):161-185.
36. Louks R, Susmel L. The linear-elastic theory of critical distances to estimate high-cycle fatigue strength of notched metallic materials at elevated temperatures. *Fatigue Fract Eng M*. 2015;38(6):629-640.
37. Peterson RE. Notch sensitivity. In: Sines G, Lwaisman J, eds. *Metal Fatigue*. New York: McGraw-Hill; 1959:293-306.
38. Neuber H. Über die Berücksichtigung der Spannungskonzentration bei Festigkeitsberechnungen. *Konstruktion*. 1968;20(7):245-251.
39. Braun M, Scheffer R, Fricke W, Ehlers S. Fatigue strength of fillet-welded joints at subzero temperatures. *Fatigue Fract Eng M*. 2020;43(2):403-416.
40. Braun M, Milaković A-S, Ehlers S, et al. Sub-zero temperature fatigue strength of butt-welded normal and high-strength steel joints for ships and offshore structures in artic regions. ASME 2020 39th International Conference on Ocean, Offshore and Arctic Engineering; June 28–July 3, 2020; Fort Lauderdale, FL, USA.
41. Kubiczek J, Herrnring H, Kellner L, Ehlers S, Diewald R. Simulation of temperature distribution in ship structures for the determination of temperature- dependent material properties. 12th European LS-DYNA Conference 2019; Koblenz, Germany
42. Braun M, Kahl A, Seidel M, Fischer C, Ehlers S. Guidance for material selection based on static and dynamic mechanical properties at sub-zero temperatures. *J Offshore Mech Arctic Eng*. 2020. submitted for publication
43. Schubnell J, Jung M, Le CH, et al. Influence of the optical measurement technique and evaluation approach on the determination of local weld geometry parameters for different weld types. *Weld World*. 2020;64(2):301-316.
44. Braun M, Milaković A-S, Andresen-Paulsen G, Fricke W, Ehlers S. A novel approach to consider misalignment effects in assessment of fatigue tests. *Ship Technol Res*. 2020. submitted for publication
45. Hobbacher AF. *Recommendations for Fatigue Design of Welded Joints and Components*. 2nd ed. Cham, Switzerland: Springer International Publishing Switzerland; 2016.
46. BS 7910:2013+A1:2015 Guide to methods for assessing the acceptability of flaws in metallic structures. 2015.
47. Lazzarin P, Lassen T, Livieri P. A notch stress intensity approach applied to fatigue life predictions of welded joints with different local toe geometry. *Fatigue Fract Eng Mater Struct*. 2003;26(1):49-58.
48. Ehlers S, Østby E. Increased crashworthiness due to arctic conditions—the influence of sub-zero temperature. *Marine Struct*. 2012;28(1):86-100.
49. Paik JK, Kim KJ, Lee JH, Jung BG, Kim SJ. Test database of the mechanical properties of mild, high-tensile and stainless steel and aluminium alloy associated with cold temperatures and strain rates. *Ships Offshore Struct*. 2017;12(sup1):S230-S256.
50. Outinen J, Makelainen P. Mechanical properties of structural steel at elevated temperatures and after cooling down. *Fire Mater*. 2004;28(2–4):237-251.
51. Wang WY, Liu B, Kodur V. Effect of temperature on strength and elastic modulus of high-strength steel. *J Mater Civil Eng*. 2013;25(2):174-182.
52. Walters CL, Alvaro A, Maljaars J. The effect of low temperatures on the fatigue crack growth of S460 structural steel. *Int J Fatig*. 2016;82:110-118.
53. Thurston KVS, Gludovatz B, Yu Q, Laplanche G, George EP, Ritchie RO. Temperature and load-ratio dependent fatigue-crack growth in the CrMnFeCoNi high-entropy alloy. *J Alloys Compd*. 2019;794:525-533.
54. Esaklul KA, Yu W, Gerberich WW. Effect of Low Temperature on Apparent Fatigue Threshold Stress Intensity Factors. In: Stephens RI, ed. *Fatigue at Low Temperatures*. West Conshohocken, PA: ASTM International; 1985;63-83. https://doi.org/10.1520/STP32747S
55. Yu W, Esaklul K, Gerberich WW. Fatigue threshold studies in Fe, Fe-Si, and HSLA steel: part II. Thermally activated behavior of the effective stress intensity at threshold. *Metall Trans A*. 1984;15(5):889-900.
56. Lucas JP, Gerberich WW. Low temperature and grain size effects on threshold and fatigue crack propagation in a high strength low alloy steel. *Mater Sci Eng A*. 1981;51(2):203-212.
57. Liao XW, Wang YQ, Qian XD, Shi YJ. Fatigue crack propagation for Q345qD bridge steel and its butt welds at low temperatures. *Fatigue Fract Eng M*. 2018;41(3):675-687.
58. Lü B, Zheng X. Predicting fatigue crack growth rates and thresholds at low temperatures. *Mater Sci Eng A*. 1991;148(2):179-188.
59. Lü B, Zheng X. A model for predicting fatigue crack growth behaviour of a low alloy steel at low temperatures. *Eng Fract Mech*. 1992;42(6):1001-1009.
60. Kim S, Jeong D, Sung H. Reviews on factors affecting fatigue behavior of high-Mn steels. *Met Mater Int*. 2018;24(1):1-14.
61. Jeong D-H, Lee S-G, Yoo J-Y, Lee J-S, Kim S. Comparative studies on near-threshold fatigue crack propagation behavior of high manganese steels at room and cryogenic temperatures. *Mater Charact*. 2015;103:28-36.
62. Jeong D, Lee S, Seo I, Yoo J, Kim S. Fatigue crack propagation behavior of Fe24Mn steel weld at 298 and 110 K. *Met Mater Int*. 2015;21(1):22-30.
63. Jung D-H, Kwon J-K, Woo N-S, Kim Y-J, Goto M, Kim S. S–N fatigue and fatigue crack propagation behaviors of X80 steel at room and low temperatures. *Metall Mater Trans A*. 2013;45(2):654-662.
64. Chai G, Johansson S. Fatigue crack propagation of super-duplex stainless steel at different temperatures. 16th European Conference of Fracture; 2006; Alexandroupolis, Greece
65. El-Shabasy AB, Lewandowski JJ. Effects of load ratio, R, and test temperature on fatigue crack growth of fully pearlitic

eutectoid steel (fatigue crack growth of pearlitic steel). *Int J Fatig*. 2004;26(3):305-309.
66. Rosenberg G. Effect of grain size on the fatigue crack growth in steels at temperatures 295 and 77 K. *ISIJ Int*. 2003;43(10): 1652-1657.
67. Aleksenko EN, Grinberg NM, Ilushchenko KA. Fatigue crack growth in KhN 60 MVYu nickel alloy at 293 and 11 K (Rost ustalostnoi treshchiny v nikelevom splave KhN 60 MVIu pri temperaturakh 293 i 11 K). Problemy Prochnosti 1988:25–31.
68. Liaw PK, Logsdon WA, Attaar MH. Computerized Near-Threshold Fatigue Crack Growth Rate Testing at Cryogenic Temperatures: Technique and Results. In: Stephens RI, ed. *Fatigue at Low Temperatures*. West Conshohocken, PA: ASTM International; 1985;173-189. https://doi.org/10.1520/STP32754S
69. Tschegg E, Stanzl S. Fatigue crack propagation and threshold in bcc and fcc metals at 77 and 293 K. *Acta Metall*. 1981;29(1): 33-40.
70. Stephens RI, Fatemi A, Lee HW, Lee SG, Vacas-Oleas C, Wang CM. Variable-Amplitude Fatigue Crack Initiation and Growth of Five Carbon or Low-Alloy Cast Steels at Room and Low Climatic Temperatures. In: Stephens RI, ed. *Fatigue at Low Temperatures*. West Conshohocken, PA: ASTM International; 1985:293-312. https://doi.org/10.1520/STP32762S
71. Yarema SY, Krasovskii AY, Ostash OP, Stepanenko VA. Development of fatigue failure of low-carbon sheet steel at room and low temperatures. *Strength Mater*. 1977;9(3):266-272.
72. Ostash OP, Kostyk EM, Levina IN. Effect of low-temperature on the initiation and growth of fatigue cracks in 08kp steel with different grain-size. *Sov Mater Sci+*. 1988;24(4):385-392.
73. Ostash OP, Zhmur-Klimenko VT. Fatigue crack growth in metals at low temperatures (a review). *Soviet Materials Science: A Transl of Fiziko-Khimicheskaya Mekhanika Materialov/-Academy of Sciences of the Ukrainian SSR*. 1987;23(2):124-135.
74. Choi HJ, Schwartz LH. Fatigue crack propagation in inter-critically tempered Fe-9Ni-0.1C and Fe-4Mn-0.15C. *Metall Trans A*. 1983;14(6):1089-1099.
75. Liaw PK, Logsdon WA. Fatigue crack growth threshold at cryogenic temperatures: a review. *Eng Fract Mech*. 1985;22(4): 585-594.
76. Fischer C. *Bewertung der Schwingfestigkeit von Schweißverbindungen mittels der Formänderungsenergiedichte*. Düren: Shaker Verlag; 2016.

How to cite this article: Braun M, Fischer C, Fricke W, Ehlers S. Extension of the strain energy density method for fatigue assessment of welded joints to sub-zero temperatures. *Fatigue Fract Eng Mater Struct*. 2020;43:2867–2882. https://doi.org/10.1111/ffe.13308